



Effects of Light Isoflurane Anesthesia on Organization of Direction and Orientation Selectivity in the Superficial Layer of the Mouse Superior Colliculus

 Masatoshi Kasai¹ and  Tadashi Isa^{1,2,3}

¹Department of Neuroscience, Graduate School of Medicine, Kyoto University, Kyoto 606-8501, Japan, ²Human Brain Research Center, Graduate School of Medicine, Kyoto University, Kyoto 606-8501, Japan, and ³Institute for the Advanced Study of Human Biology (WPI-ASHBi), Kyoto 606-8501, Japan

The superior colliculus (SC) is the midbrain center for integrating visual and multimodal sensory information. Neurons in the SC exhibit direction and orientation selectivity. Recent studies reported that neurons with similar preferences formed clusters in the mouse SC (Ahmadlou and Heimel, 2015; Feinberg and Meister, 2015; de Malmazet et al., 2018; Li et al., 2020). However, it remains controversial as to how these clusters are organized within the SC (Inayat et al., 2015; Chen et al., 2021). Here, we found that different brain states (i.e., awake or anesthetized with isoflurane) changed the selectivity of individual SC neurons and organizations of the neuronal population in both male and female mice. Using two-photon Ca^{2+} imaging, we examined both individual neuronal responses and the spatial patterns of their population responses. Under isoflurane anesthesia, orientation selectivity increased and a larger number of orientation-selective cells were observed when compared with the awake condition, whereas the proportions of direction-selective cells were similar in both conditions. Furthermore, direction- and orientation-selective cells located at closer positions showed more similar preferences, and cluster-like spatial patterns were enhanced. Inhibitory responses of direction-selective neurons were also reduced under isoflurane anesthesia. Thus, the changes in the spatial organization of response patterns were considered to be because of changes in the balance of excitation and inhibition, with excitation dominance, in the local circuits. These results provide new insights into the possibility that the functional organization of feature selectivity in the brain is affected by brain state.

Key words: direction selectivity; functional architecture; isoflurane; orientation selectivity; superior colliculus; two-photon imaging

Significance Statement

Recent large-scale recording studies are changing our view of visual maps in the superior colliculus (SC), including findings of cluster-like localizations of direction- and orientation-selective neurons. However, results from several laboratories are conflicting regarding the presence of cluster-like organization. Here, we demonstrated that light isoflurane anesthesia affected the direction- and orientation-tuning properties in the mouse superficial SC and that their cluster-like localization pattern was enhanced by the anesthesia. Furthermore, the effect of anesthesia on direction selectivity appeared to be different in the excitatory and inhibitory populations in the SC. Our results suggest that the functional organization of direction and orientation selectivity might be regulated by the excitation–inhibition balance that depends on the brain state.

Received June 9, 2021; revised Nov. 18, 2021; accepted Nov. 22, 2021.

Author contributions: M.K. and T.I. designed research; M.K. performed research; M.K. contributed unpublished reagents/analytic tools; M.K. analyzed data; M.K. and T.I. wrote the paper.

This study was supported by Grants-in-Aid for Scientific Research (C) 19K06940, The Futaba Foundation, and Konica Minolta Science and Technology Foundation to M.K.; and Grant-in-Aid for Scientific Research (A) 19H01011 to T.I. We thank Professor B. Lowell (Beth Israel Deaconess Medical Center, Boston, MA) and Dr. R. Yamamoto (Kanazawa Medical University, Kahoku, Japan) for providing Vgat-ires-Cre knock-in mice. We also thank Dr. R. Veale (Kyoto University, Kyoto, Japan) for critical reading of the manuscript.

The authors declare no competing financial interests.

Correspondence should be addressed to Masatoshi Kasai at kasai.masatoshi.2s@kyoto-u.ac.jp.

<https://doi.org/10.1523/JNEUROSCI.1196-21.2021>

Copyright © 2022 the authors

Introduction

The superior colliculus (SC) is an evolutionarily old center that integrates visual and other sensory information to initiate a variety of visually driven behaviors, including orienting and avoidance (Hoy et al., 2019; Shang et al., 2019; Isa et al., 2020; for review, see Basso et al., 2021; Isa et al., 2021). Furthermore, visual processing in the SC has been attracting greater attention for understanding the mechanisms of subcortical vision and related visually evoked behaviors, partly because recent human studies have suggested that the SC processes more complex visual features, such as fearful stimuli and faces (de Gelder et al., 2005; Ajina et al., 2020).

The superficial layer of the SC (sSC) receives retinotopically organized visual input directly from retinal ganglion cells. Recent advances in imaging technology have enabled us to acquire detailed spatial information with single-cell resolution about the tuning properties of neuronal populations in the SC. For example, we used very small visual stimuli (diameter, 0.5–1°; Kasai and Isa, 2016) and demonstrated retinotopic organization in the sSC, which had also been shown by electrophysiological and other imaging techniques (Dräger and Hubel, 1976; Mrcic-Flogel et al., 2005). Retinotopic organization is a fundamental architecture conserved across various regions of the visual system. In the primary visual cortex (V1) in higher mammals, multiple types of functional architectures, such as ocular dominance columns and orientation columns, overlap on the retinotopic map, composing a complex pattern of functional organizations. The cluster-like organization is considered to benefit a higher level of information processing in general (Newman, 2006). In rodent V1, the retinotopic organization is conserved, while organizations representing orientation or motion direction columns are absent (Ohki et al., 2005). On the other hand, several groups recently reported functionally organized response properties in the rodent SC. For example, neurons with direction and orientation selectivity formed columnar or patchy clusters (Ahmadlou and Heimel, 2015; Feinberg and Meister, 2015; Li et al., 2020), although they were not observed in V1. Furthermore, direction-selective (DS) cells tuned to temporal direction were found in the binocular region of the sSC, while nasally tuned DS cells were distributed in its monocular region (de Malmazet et al., 2018). These findings suggest that the SC might play more important roles in visual perception than previously considered in rodents. However, the cluster-like patterns of tuning properties are different from the stereotypic columnar structures found in the V1 of higher mammals. Furthermore, several other studies reported inconsistent patterns of such functional clusters (Inayat et al., 2015; Chen et al., 2021).

Neural responses to specific sensory stimuli can be different under different brain states including general anesthetics (Chen and Song, 2019). In the sSC, recent physiological recordings conducted in the awake condition (Feinberg and Meister, 2015; de Malmazet et al., 2018) or while anesthetized with urethane (Ahmadlou and Heimel, 2015) showed that wakefulness and some anesthetics did not affect direction and orientation selectivity (Chen et al., 2021). Isoflurane (iso), however, which is a widely used general anesthetic, has been known to change not only firing patterns of individual neurons, but also the function of local circuit or brain-wide network activities (Goltstein et al., 2015; Bukhari et al., 2018; Zhang et al., 2020). In this study, to clarify whether isoflurane affects the tuning properties of neurons in the sSC, we tested both direction and orientation tuning of neuronal populations in mouse sSC using two-photon Ca^{2+} imaging and compared spatial patterns of those tuning properties under awake and anesthetized conditions. We further examined the effects of isoflurane on GABAergic sSC neurons, because their inhibitory interactions were shown to be critical in regulating orientation selectivity in V1 (Priebe and Ferster, 2005) as well as in integrating excitatory inputs from the lateral geniculate nucleus (Reid and Alonso, 1995; Jin et al., 2011). Our results suggested that the functional architecture of the sSC, which has been considered to be a stable circuit, can be dynamically modulated by the different brain states.

Materials and Methods

All mice were handled in accordance with the *Regulation on Animal Experimentation at Kyoto University* and the National Institutes of Health *Guide for the Care and Use of Laboratory Animals*. All experimental procedures were approved by the Kyoto University Animal Care and Users Committee and the Kyoto University Safety Committee for Recombinant DNA Experiments.

Animal preparation. Ten C57BL/6 mice of both sexes (age range, 6–15 weeks) were used. To express the GCaMP calcium sensor protein in neurons in the SC, the adeno-associated virus (AAV) vector carrying GCaMP [AAV1-hSyn-GCaMP6f, $\sim 1.1 \times 10^{12}$ viral genomes (vg)/ml] was injected into the sSC. Six Vgat-ires-Cre knock-in mice (Vong et al., 2011) and the Cre-dependent AAV vector (AAV1-hSyn-Flex-GCaMP6f, $\sim 0.4 \times 10^{13}$ vg/ml) were selected for Cre-dependent GCaMP expression specifically in inhibitory neurons. pAAV-Syn-GCaMP6f-WPRE-SV40 (viral prep #100837-AAV1, Addgene; <http://n2t.net/addgene:100837//>; BRID:Addgene_100837) and pAAV-Syn-Flex-GCaMP6m-WPRE-SV40 (viral prep #100838-AAV1, Addgene; <http://n2t.net/addgene:100838//>; BRID:Addgene_100838) were gifts from Douglas Kim and the GENIE Project (Chen et al., 2013).

Before AAV injection, mice were anesthetized with isoflurane (3% for induction and 1–2% for maintenance), dexamethasone (0.2 mg/kg, i.m.), and carprofen (5 mg/kg, i.m.) were administered. A heating pad was used to maintain body temperature at 37°C. A custom-made titanium head plate was placed on the skull and glued with dental adhesive resin cement (Super-Bond, Sun Medical). A chronic imaging window was implanted over the right side of the occipital cortex. A craniotomy was made by drilling (1.5 mm lateral and anterior from λ) and removing a portion of the skull. To expose the surface of the sSC, the mediocaudal part of the overlying cortices was aspirated after cutting the dura. During the aspiration, the brain was rinsed with brain buffer (135 mM NaCl; 5.4 mM KCl; 1.0 mM MgSO_4 ; 5.0 mM HEPES, pH 7.4) until the bleeding stopped. The AAV vector was injected into the SC at three to five sites (~ 600 nl/site) ~ 100 μm from the surface using a glass pipette. A small glass cube (length, 1.4 mm; width, 1.3 mm; thickness, 0.8–1.2 mm; NITTO OPTICAL Co., LTD.) was attached with a circular cover glass (φ 4 mm; Matsunami Glass) using optical adhesive (catalog #81, Norland Optical) to make a “glass plug.” The glass plug was placed on the surface of sSC, and the edges of the coverslip were sealed with instant glue and cemented in place. In this surgery, both the central and transverse sinuses were left intact. Also, we tried to limit the removal of V1 to as little as possible (Fig. 1a). Mice were given 3–4 weeks to recover, and GCaMP was expressed before the start of the *in vivo* calcium imaging experiments.

In vivo imaging, visual stimulation, and eye tracking. *In vivo* calcium imaging was conducted using a two-photon laser-scanning microscope (model FV1000MPE, Olympus). GCaMP was excited with a wavelength of 920 nm (Mai Tai, DeepSee) through a 25 \times , 1.05-NA (numerical aperture) objective (model XLPLNX25WMP2, Olympus). Mice were put on a rotatable cylinder (Fig. 1b) under the objective lens with their head fixed to the head plate. Two-photon imaging was performed from the superficial layer of the SC in a range of 10.0–244.85 μm (median, 67.39 μm) in depth, and a 320 \times 320 pixels image was scanned at ~ 4 Hz.

Visual responses were first obtained under awake conditions, then anesthesia was induced with 3% isoflurane, and chlorprothixene was administered for further sedation (1 mg/kg BW (Body Weight), i.p.). After reducing the concentration of isoflurane to 0.8% and waiting for >30 min, visual responses under isoflurane anesthesia were obtained from nearly identical neural populations (Fig. 1d). As the response characteristics of each region of interest (ROI) recorded at intervals of ≥ 30 min did not change, the recordings were considered to be stable in the same imaging plane at different times (Fig. 1f,g).

Visual stimuli were generated by Psychtoolbox3 (Brainard, 1997) and presented on an LCD screen (model P190S19, DELL). When presenting moving-bar stimuli, the position of the LCD monitor was adjusted to match the visual response center of the imaged population and the center of the LCD monitor. A moving white bar on a black background was used to examine the direction and orientation selectivity of sSC neurons. The bar stimuli were 3° in width and moved perpendicular

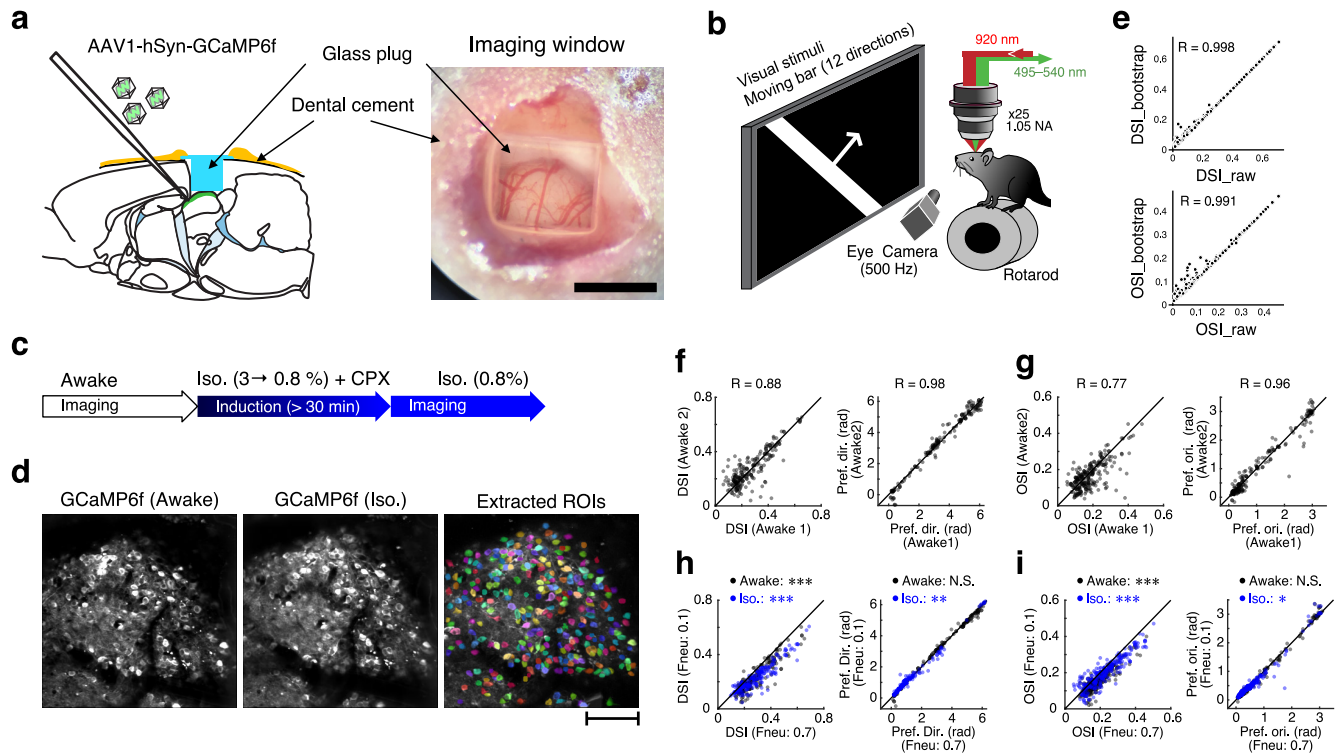


Figure 1. Mouse preparation and experimental setup. **a**, Sagittal view of the mouse brain (left) and dorsal view of the sSC surface through the cranial window (right). Scale bar, right, 1 mm. **b**, Experimental setup. The mouse was placed on a rotarod with its head fixed under the objective lens. Moving-bar stimuli were presented to the left eye of the mouse. Eye movements were recorded at a frame rate of 500 Hz. **c**, Time course of imaging and isoflurane anesthesia. **d**, Example images of GCaMP-expressing neurons in the sSC during awake (left), isoflurane (middle), and extracted ROIs (right). Colors of individual ROIs are randomly assigned. Scale bar, 100 μ m. **e**, Comparisons of DSI (top) and OSI (bottom) calculated from the raw data (horizontal axis) and bootstrapped data (vertical axis). **f**, **g**, Stability of imaging results: DSI (left) and preferred direction (right) of DS and weak DS cells (see Materials and Methods) of neurons recorded in the same imaging site with >30 min interval (**f**); OSI (left) and preferred orientation (right) of OS and weak OS cells (**g**). **h**, **i**, Effects of neuropil contamination tested by changing the factor of neuropil contamination (0.7; current analysis vs 0.1; see Materials and Methods). Similar to **f** and **g**, the DSI of the recorded cell within the same imaging site (**h**, left), preferred direction of DS and weak DS cells (OSI (**i**, left), and preferred orientation of OS and weak OS cells (**i**, right) are plotted. In **e–i**, pairwise correlation coefficients (R) are shown in each panel. In **f–i**, black dots indicate the neurons recorded in the awake condition, and blue dots indicate the data from the isoflurane condition. N.S.: not significant.

to the bar orientation at a speed of 10° /s. One of 12 directions (each separated by 30°) was randomly selected and moved from one edge to the opposite edge of the screen in ~ 11 s. Ten to 12 repetitions in each direction were tested for analysis of direction and orientation selectivity. Interstimulus intervals were fixed at ~ 10 s (Fig. 1b).

Eye movements of the stimulated eye were monitored during the recording, using two CMOS Cameras (Grasshopper3 USB3, TELEDYNE FLIR) at 500 Hz. Fast and slow drifts of the pupil center, including saccade-like eye movements, were tracked by iReCHS2 software (Matsuda et al., 2017). No optokinetic reflexes (OKRs) were induced by the moving-bar stimulation. Trials in which the eye position moved considerably during the experiments or saccade-like movements occurred during visual stimuli were omitted from the analysis.

Data analysis. Brain motion during the two-photon imaging was corrected by Non-Rigid Motion Correction programs (Pneumatikakis and Giovannucci, 2017) and/or Suite2P (Pachitariu et al., 2017). ROIs were first detected using Suite2P and were manually corrected if needed. The mean fluorescence change in each ROI [$F(t)$] was normalized by the prestimulus baseline (F_0), $\Delta F/F_0 = (F(t) - F_0)/F_0$. Signals from the neuropil surrounding ROIs may mask the signal from neurons and thus underestimate the selectivity (Fig. 1h,i). Therefore, neuropil contaminations were corrected by subtracting surrounding neuropil signals (factor of 0.7). When the peak amplitude of $\Delta F/F_0$ was less than the baseline level (mean + 2 SDs), those neurons were treated as no-response cells. The peak responses to each moving direction or bar orientation were analyzed for estimating the tuning properties.

To quantify the direction and orientation selectivity, we first computed the direction selectivity index (DSI) and the orientation selectivity index (OSI) of each neuron by calculating the circular mean of the peak

responses, $R(\theta)$, at each moving-bar direction (θ) using the following equations:

$$DSI = \frac{\sum_{\theta} R(\theta) \exp(i\theta)}{\sum_{\theta} R(\theta)}, \quad OSI = \frac{\sum_{\theta} R(\theta) \exp(i2\theta)}{\sum_{\theta} R(\theta)}.$$

Because of the small size of our datasets (10–12 repetitions for each direction), we resampled the data using bootstrap methods (5000 times) and computed the median of each index from the bootstrapped distribution (Mazurek et al., 2014; Chang and Fitzpatrick, 2021). Bootstrapped medians of the DSI and OSI were not different from those calculated from the raw dataset (Fig. 1e). DSIs and OSIs between 0.1 and 0.3 were used as threshold levels for the direction- and orientation-selective neurons in previous studies (Feinberg and Meister, 2015; Inayat et al., 2015; Li et al., 2020). Based on these criteria and the distribution of our data, we set up the following criteria to compare our results and the previous reports: when the bootstrapped DSI was >0.2 or the bootstrapped OSI was >0.15 , we selected those cells as candidate cells that were selective for the moving-bar direction or bar orientation. We further analyzed the selected candidate cell to evaluate its DS and orientation-selective (OS) tuning properties by Bayesian inference with response models. We tested two models. One is the sum of two von Mises (VM) functions (Anzai et al., 2007; Sadeh and Rotter, 2015) as Equation 1. $I_0(\kappa)$ in Equation 2 is the modified Bessel function of the first kind with order 0. In this model, neuronal responses of a given cell are inferred as the sum of unimodal and bimodal VM functions with noise (σ). The other is the constant response model (Eq. 3) for nonselective responses, which is independent of the direction or orientation of the stimuli, as follows:

$$\text{Model}_1 = p * \text{VM}(\kappa_1, \theta) + (1 - p) * \text{VM}(\kappa_2, \theta + \pi) + \sigma \quad (1)$$

$$\text{VM}(\kappa, \theta) = \frac{\exp(\kappa * \cos(\theta - \theta_0))}{2\pi I_0(\kappa)} \quad (2)$$

$$\text{Model}_2 = \mu + \sigma. \quad (3)$$

Using Markov chain Monte-Carlo (MCMC) simulations, posterior distributions of the following parameters were obtained for each cell, as follows: p (proportion of the first VM component), θ_0 (preferred direction), and κ (concentration parameter of the VM function) in Model₁. The parameter of μ in Model₂ is the mean response amplitude for nonselective tuning. The MCMC sampling was performed using the R and *rstan* package (Stan Development Team, 2020). Four chains of 4000 simulated draws from the posterior were sampled. The simulated draws were preceded by 1000 “burn-in” draws, which were not included in the posterior. Each MCMC chain was thinned by including only every second draw. Values of R^{\wedge} equaled 1.0 for all parameters, indicating convergence across the four chains initiated from disparate starting values. By comparing the widely applicable information criteria [WAICs (Watanabe, 2010)] of the two models, we chose the better response model for that cell. When the bootstrapped DSI or OSI was higher than the threshold (DSI ≥ 0.2 , OSI ≥ 0.15) and Model₁ was selected, those neurons were defined as DS or OS cells. When the bootstrapped DSI or OSI was smaller than the threshold but the neuron was selected by the Model₁, those neurons were treated as weak DS or weak OS cells. Last, when Model₂ was selected, those neurons were treated as nonselective cells.

To compare the changes in preferred direction and orientation of selective and weakly selective cells during the awake and isoflurane conditions, circular correlation coefficients were calculated (see Fig. 5*a,b*). Angular statistics were tested using the *circular* package (Agostinelli and Lund, 2017) in R (<https://r-forge.r-project.org/projects/circular/>).

Retinotopic locations of individual imaging sites were estimated by the distribution of receptive-field centers of nonselective neurons in the field of view. The location of the stimulus on the monitor was extracted at the response onset when the amplitude of $\Delta F/F_0$ exceeded the mean \pm SD level in 12 directions. The center of the receptive field (RF) was estimated as the centroid of these points (Fig. 2*g-i*).

In figures, statistical differences are indicated as N.S. * $p < 0.05$, ** $p < 0.01$, and *** $p < 0.001$. The Wilcoxon signed-rank (WSR) test was used for comparing paired samples. Distributions of DSI and OSI were compared using the Kolmogorov–Smirnov (KS) test. All statistics are represented as the mean \pm SD. In analyzing the angular data, we calculated their circular mean and SD. The box plots in Figure 3 (see also Figs. 6, 7, 8) show the median, 25th percentile, and 75th percentile of the data.

Results

Tuning properties of sSC neurons are affected by isoflurane anesthesia

Using two-photon Ca^{2+} imaging techniques, we recorded the direction- and orientation-tuning properties of individual neurons and their populations from the sSC during different brain states: awake and under light anesthesia with isoflurane (0.8%).

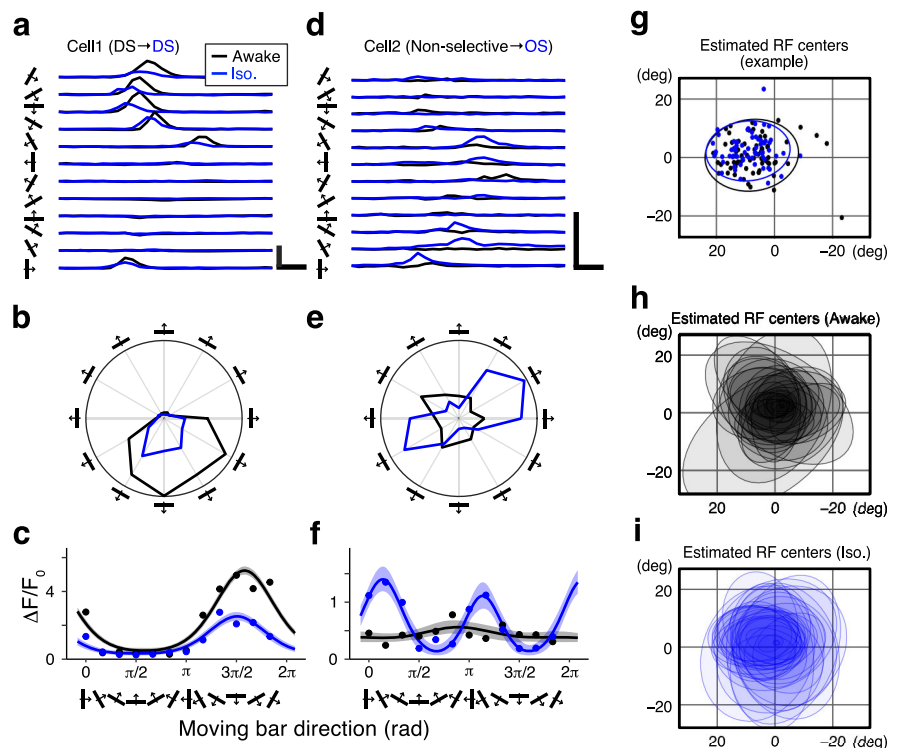


Figure 2. Effects of isoflurane anesthesia on two example sSC neurons. Black and blue dots, lines, and hatched areas indicate the records during the awake condition and isoflurane anesthesia, respectively. **a**, Mean Ca^{2+} responses of a DS cell to 12 moving-bar stimuli with different directions. Calibration: 5 $\Delta F/F_0$, 2 s. **b**, Polar plots based on the peak Ca^{2+} responses. **c**, Fitted VM models by Bayesian inference (lines). Shaded areas indicate 95% credible intervals of the models. Dots indicate the bootstrapped median of the peak $\Delta F/F_0$ responses to each direction of moving-bar stimuli. **d–f**, Another example cell that exhibited nonselective responses during the awake state and was orientation selective during anesthesia, using the same format as **a–c**. **g–i**, Estimated RF centers: RF centers of individual neurons (dots) in an example imaging site and their distributions indicated by the normal data ellipses (**g**); and ellipses of the RF centers from 34 imaging sites in the awake condition (**h**) and under isoflurane anesthesia (**i**).

After expressing GCaMP6f in the sSC neurons of wild-type mice, we recorded responses from a total of 5801 visually responding neurons in 35 imaging sites in the sSCs of 10 mice. To compare the direction and orientation tuning of individual neurons, we first recorded the neuronal population responses in the awake condition under head-fixed conditions. Then, isoflurane was introduced and, after waiting ~ 30 min, recordings were performed from the same optical plane under the following conditions. Moving-bar stimuli with 12 possible directions were pseudorandomly presented. Ca^{2+} responses toward each direction were averaged after removing the trials with saccade-like or large eye movements including blinks. Isoflurane anesthesia affected neuronal responses to the moving-bar stimuli, and these effects varied from neuron to neuron. Ca^{2+} responses and the tuning properties of two example sSC neurons are shown in Figure 2*a–f*. Cell 1 exhibited similar direction selectivity in both the awake and anesthetized states (DSI, 0.58 vs 0.50; OSI, 0.12 vs 0.13; awake vs iso; Fig. 2*a–c*). The peak amplitude was reduced by iso, while the preferred directions in the awake and isoflurane conditions were similar (4.99 vs 4.83 radian (rad); awake vs iso). Another example cell (Cell 2) is shown in Figure 2*d–f*. This neuron showed no strong selectivity for either stimulus direction or orientation in the awake condition and was therefore classified as a nonselective type. However, during isoflurane anesthesia, it did exhibit orientation selectivity (DSI, 0.11 vs 0.12; OSI, 0.06 vs 0.43; awake vs iso). The peak time points of the maximum Ca^{2+} responses differed depending on the angle of the moving-bar

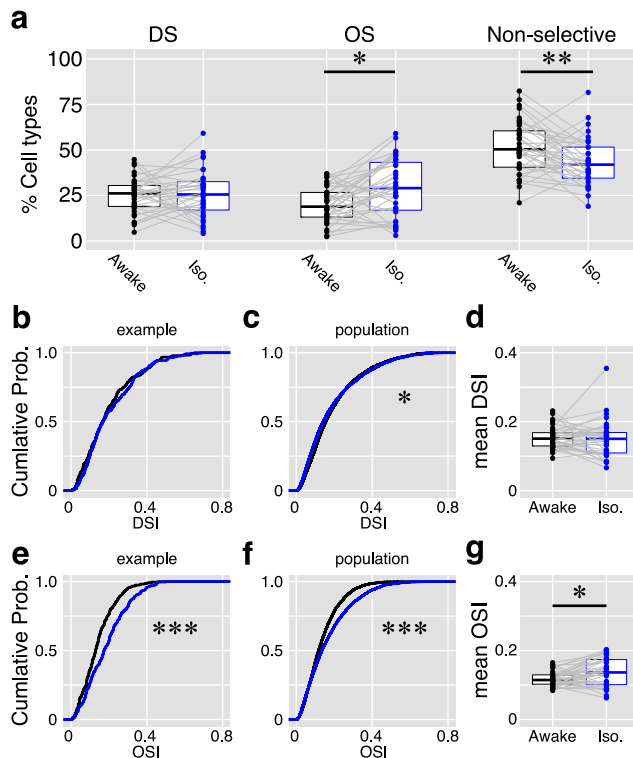


Figure 3. Summary of isoflurane effects on direction and orientation responses. *a*, Proportions of DS cells, OS cells, and nonselective cells in the awake (black) and anesthetized (iso; blue) states. Dots indicate the data from each imaging site ($n = 35$ sites). *b–d*, Changes in the DSI. *b*, A cumulative probability of DSI of 214 cells in an example imaging site. *c*, A cumulative probability of DSI of 5801 neurons from all the 35 imaging sites. *d*, Comparisons of mean DSIs. Dots indicate the mean DSIs of individual imaging sites ($n = 35$ sites). *e–g*, Changes in OSI are shown with cumulative probabilities and paired comparison of mean OSIs, as in *b–d*. Gray lines in *a*, *d*, and *g* connect the data from the same imaging site.

stimuli (Fig. 2*a–d*), possibly because the receptive fields of most neurons were off-centered in the LCD monitor in the present experimental condition. To estimate the RF center of each neuron, we calculated the mean of location of the stimulus at the response onset for the 12 directions. Figure 2*g* shows the distribution of RF centers of the nonselective neurons in an example imaging site, represented by a normal ellipse. As shown in the figure, the RF centers most overlapped between the awake and isoflurane conditions in this case. Figure 2, *h* and *i*, shows the distributions of RF centers in all 35 experiments under awake and isoflurane conditions, respectively. These results indicate that most of the RF centers in all the experiments were included in the LCD monitor. Furthermore, isoflurane may slightly alter the latency of moving-bar responses and, accordingly, the RF locations might have been somewhat shifted; however, the overall RF areas were similarly distributed around the center of the LCD monitor throughout the experiments.

To examine whether isoflurane anesthesia changes the number of direction- and orientation-selective cells and their tuning strengths at the population level, we analyzed the proportion of DS cells, OS cells, and nonselective cells in each imaging site and compared their properties before and after isoflurane (Fig. 3*a*). The mean proportions of DS cells from the 35 imaging sites were similar in both conditions ($25.2 \pm 9.6\%$ vs $25.8 \pm 13.0\%$; awake vs iso, $p = 0.44$, WSR test). However, the proportion of OS cells was higher ($20.1 \pm 9.9\%$ vs $29.2 \pm 16.0\%$; awake vs iso, $p = 0.0018$) and that of nonselective cells was lower ($51.5 \pm 14.5\%$ vs $43.2 \pm 13.2\%$; awake vs iso, $p = 0.006$) during anesthesia. The

number of DS and OS cells depended on the criteria used to classify cells as DSI and OSI ($\text{DSI} \geq 0.2$, $\text{OSI} \geq 0.15$); therefore, we further compared the changes in DSI and OSI of individual neurons in each imaging site. Cumulative distributions of the DSI and OSI of 260 neurons recorded in an example imaging site and of the total 5801 neurons are plotted in Figure 3, *b* and *e*. Similar to the proportions of DS and OS cells, the distributions of the DSIs were not different in the awake and anesthetized states ($p = 0.22$, KS test; Fig. 3*b*), while the OSIs were larger during isoflurane ($p = 4.69 \times 10^{-7}$; Fig. 3*e*). The same tendencies were observed when all 5801 cells were analyzed (DSI, $p = 0.002$; OSI, $p = 2.2 \times 10^{-16}$; Fig. 3*c*, *f*). To account for individual differences among mice and neurons, mean DSIs and OSIs for each imaging site were compared both in the awake and isoflurane conditions. The mean DSI was not affected by isoflurane (0.15 ± 0.03 vs 0.15 ± 0.06 ; awake vs iso, $p = 0.39$; Fig. 3*d*), while the mean OSI was significantly higher in the anesthetic condition (0.12 ± 0.02 vs 0.14 ± 0.04 ; awake vs iso, $p = 0.01$; Fig. 3*g*). These results suggest that isoflurane anesthesia increases the orientation selectivity of sSC neurons at the population level.

The proportion of DS cells and the distribution of DSIs were similar at the population level in both conditions; however, the effect of isoflurane was considerably varied at the individual neuronal level. In Figure 4*a*, 281 cells in an example imaging site were analyzed; 82 cells showed direction selectivity in the awake condition (Fig. 4*a*, left), and a similar number of DS cells ($n = 90$) were found in the isoflurane condition (Fig. 4*a*, right); however, many of these were not the same cells. Their approximate preferred directions are indicated with red circles. Here, the preferred directions of the DS cells in the awake condition were different from those during the isoflurane condition. Many DS cells exhibited reduced selectivity and were weak DS cells (see Materials and Methods), or non-DS [$n = 47$ from 82 DS cells in awake condition (57.3%)]. Moreover, many non-DS cells in the awake condition were DS cells after anesthesia [$n = 60$ of 182 non-DS cells in awake condition (33.0%)]. The OS cells observed in the same imaging site are shown in Figure 4*b*. As shown in Figure 3, the number of OS cells was larger in the isoflurane condition (awake vs iso, 68 vs 114). In Figure 3, the preferred orientations are indicated by open blue circles. The preferred orientations of the OS cells in the awake condition were markedly different after isoflurane anesthesia. Some of the OS cells in the awake condition were non-OS [$n = 30$ of 68 OS cells (44.1%)] after anesthesia, and some of the non-OS cells in the awake condition were OS cells after anesthesia [$n = 72$ of 196 non-OS cells (36.7%)].

The direction and orientation selectivity of individual neurons were quite different across awake and isoflurane conditions. Figure 4*c* shows a summary of changes in response selectivity before and after the anesthesia. In the isoflurane condition, 1440 neurons were defined as DS cells, of which 365 were originally DS cells (25.4%; Fig. 4*c*, red) and 302 were originally OS cells (21.0%; Fig. 4*c*, blue) in the awake condition. Most of them (39.8%) were weakly selective cells (Fig. 4*c*: weak DS: 264 cells, pink; weak OS cells: 309 cells, light blue). Similarly, 1650 cells were OS in the isoflurane conditions. While 21.8% (360 cells) were OS cells and 20.3% (335 cells) were DS cells in the awake condition, most of them were weakly selective cells (42.3%; weak DS, 319 cells; weak OS, 379 cells). Furthermore, of 817 weak DS and 1063 weak OS cells in the isoflurane condition, 21.3% (174 cells) and 14.8% (158 cells) exhibited increased selectivity (weak

DS to DS and weak OS to OS, respectively). However, most of them were also originally weakly selective cells (weak DS and weak OS) in the awake condition.

To examine how selectivity was changed by isoflurane, we compared the DSIs of DS and weak DS cells. There was no significant correlation in the changes of DSIs before and after anesthesia, even for the DS cells in both conditions (Fig. 4*d*). For changes in OSIs, there was also no significant correlation before and after anesthesia (Fig. 4*e*). We also examined the changes in their preferred direction or orientation before and after isoflurane anesthesia (Fig. 5). While some neurons showed similar tuning properties during awake and isoflurane conditions, there were diverse changes in their preferences. Thus, it was difficult to draw clear conclusions about the effects of isoflurane on individual neurons. Therefore, we then focused on the effects of isoflurane on the neuronal population, rather than on preference changes in individual neurons.

Increases in local response similarity during isoflurane anesthesia

Recent imaging studies revealed topographic organizations of DS cells and OS cells in the sSC, consisting of columnar or horizontal patchy patterns (Ahmadlou and Heimel, 2015; Feinberg and Meister, 2015; de Malmazet et al., 2018; Li et al., 2020). We also examined the relationships between the locations of selective neurons and their preferred directions and orientations, and whether any spatial organization was altered by isoflurane.

Figure 6, *a* and *b*, shows the locations of DS cells projected onto the imaging field of view. The preferred directions of individual DS cells are indicated by the direction of arrows and the colors of the ROIs. In the awake condition, there was no clear systematically organized functional architecture of the DS cells (Fig. 6*a,b*, left panels). However, during isoflurane anesthesia, the direction tuning pattern of DS cells appeared to be more locally aligned (Fig. 6*a,b*, right panels). To measure the local similarities of preferred directions, we calculated the differences in the preferred directions of all pairs of DS cells recorded in the same field of view. We also tested the randomness of the clustering pattern by comparing it with a simulated dataset using shuffled data from the awake state. 2-D histograms of differences in preferred direction were then plotted as a function of the paired distance of all possible neuronal combinations (Fig. 6*e*). In a comparison of the awake data with the randomized (RND) dataset, there was a small but highly significant difference for DS cells that were located within 100 μm of each other. On the other hand, there was no significant difference from the randomized data for DS cells that were 100–200 or 200–300 μm distant from one another [Fig. 6*g*: RND (green) vs awake (black); 0–100 μm : 1.58 vs 1.43 rad, $p = 1.2 \times 10^{-4}$, $n = 34$; 100–200 μm : 1.59 vs 1.54 rad, $p = 0.12$, $n = 34$; 200–300 μm : 1.54 vs 1.56 rad, $p = 0.86$, $n = 34$, WSR test]. Furthermore, comparing preferred directions of DS cells during the awake and iso conditions showed that DS cells exhibited stronger clustering patterns during the isoflurane condition [Fig. 6*g*: awake (black) vs iso (blue); 0–100 μm : 1.43 vs 1.07 rad, $p = 0.006$, $n = 34$; 100–200 μm : 1.54 vs 1.33 rad, $p = 6.2 \times 10^{-5}$, $n = 35$; 200–300 μm : 1.56 vs 1.29 rad, $p = 0.014$, $n = 33$; WSR test].

The locations of OS cells and their preferred orientations are shown in Figure 6, *c* and *d*. A prominent cluster of OS cells with similar preferred orientations was observed during the isoflurane condition. The local similarity of these differences was analyzed as was that for the DS cells. Compared with a random distribution, a clustered localization of OS neurons with similar

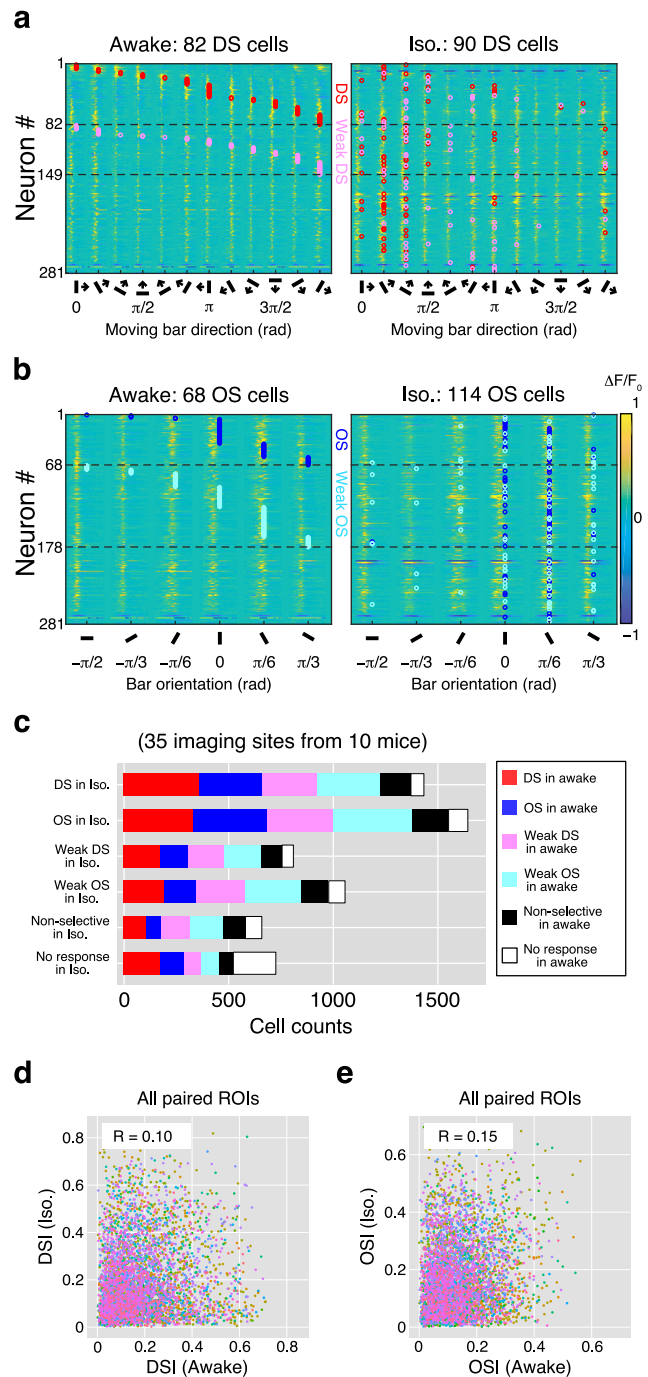


Figure 4. Changes in response patterns of individual neurons. **a**, Color maps show the averaged Ca^{2+} responses to 12 moving-bar stimuli of 281 neurons recorded from an example imaging site. Each line indicates an individual neuronal response during awake (left) and isoflurane (right) conditions. The order of the neurons (“Neuron #”) is the same in both panels. DS cells and weak DS cells are separated by dotted lines. The preferred direction of each DS and weak DS cell is labeled with red and pink circles, respectively. **b**, OS responses are illustrated as in **a** for the DS responses. The preferred orientation of each OS and weak OS cell are labeled with blue and cyan circles, respectively. The amplitude of $\Delta F/F_0$ in **a** and **b** is color coded according to the color bar on the right in **b**. **c**, Summary of the changes in six response types (DS, OS, weak DS, weak OS, nonselective, and no response) from awake to anesthetic condition. **d**, Changes in the DSI of individual DS or weak DS cells, shown by plotting the indices in the awake condition on the horizontal axis and those in the isoflurane condition on the vertical axis. Each dot indicates an individual neuron. Colors of dots indicate the individual imaging sites ($n = 35$). The value of the correlation coefficient (R) is inserted in each panel. **e**, Change in OSI of individual OS or weak OS cells as shown in **d**.

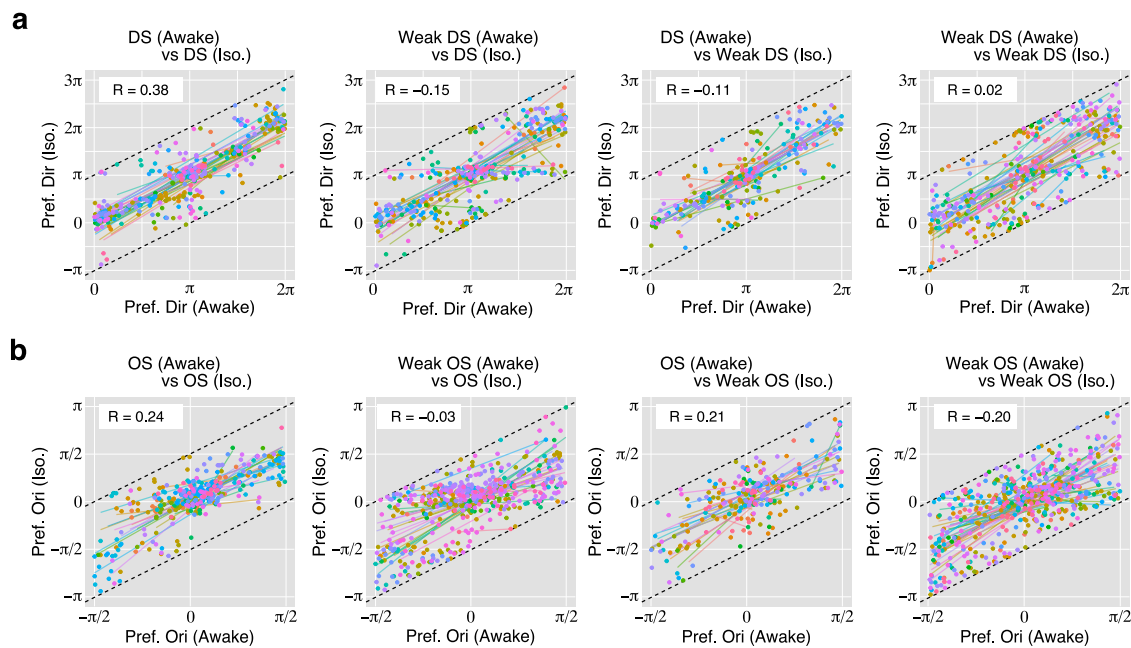


Figure 5. Changes in preferred directions and orientations of DS and OS cells. **a**, Changes in preferred directions of individual DS or weak DS cells, shown by plotting the preferred angles in the awake condition on the horizontal axis and those in the isoflurane condition on the vertical axis. Each dot indicates an individual neuron. Each dot is moved so that the difference of the angle between awake and iso conditions is less than π (rad). Dotted lines indicate the range of data wrapping. Colors of dots indicate the individual imaging sites. Lines with different colors indicate the regression lines for data from each imaging site. The value of circular correlation (R) is inserted in each panel. **b**, Changes in the preferred orientation of individual OS or weak OS cells are shown as in **a**. Each dot is moved so that the difference of the angle between awake and iso conditions is less than $\pi/2$ (rad).

orientation selectivity was observed during the awake condition [Fig. 6*h*: randomized (green) vs awake (black); 0–100 μm : 0.79 vs 0.60 rad, $p = 1.4 \times 10^{-6}$, $n = 34$; 100–200 μm : 0.78 vs 0.63 rad, $p = 1.5 \times 10^{-4}$, $n = 34$; 200–300 μm : 0.78 vs 1.56 rad, $p = 0.0021$, $n = 34$; WSR test]. Similar to the DS cells, the local similarities of OS cells were higher during the isoflurane condition than the awake conditions [Fig. 6*h*: awake (black) vs iso (blue); 0–100 μm : 0.60 vs 0.39 rad, $p = 5.0 \times 10^{-7}$, $n = 34$; 100–200 μm : 0.64 vs 0.49 rad, $p = 6.2 \times 10^{-5}$, $n = 34$; 200–300 μm : 0.67 vs 0.52 rad, $p = 9.9 \times 10^{-3}$, $n = 34$; WSR test; Fig. 6*h*].

Direction selectivity is specifically reduced in inhibitory sSC neurons by isoflurane

One of the effects of isoflurane is known to be the activation of GABA_A receptors (Topf et al., 2003; Bieda et al., 2009). Nearly half of the neurons in the sSC are GABAergic inhibitory neurons (Mize, 1988; Behan et al., 2002). Therefore, disruption of this inhibitory network in the sSC might be responsible for the above results. Furthermore, understanding the cell type specificity of the observed functional organization is important to understand the circuit mechanisms of direction/orientation selectivity in the SC. In V1, local inhibitory networks are critical for regulating orientation-selective responses (Priebe and Ferster, 2005). However, whether the effects of anesthesia on direction and/or orientation selectivity varies between excitatory and inhibitory neurons in the SC is unclear. Therefore, we next focused on the inhibitory neurons in the sSC and the effects of isoflurane anesthesia on their tuning responses to moving-bar stimuli. To target the inhibitory neurons specifically, Vgat-ires-Cre knock-in mice were used. The Cre-dependent AAV vector was injected into the sSC to express GCaMP6f in inhibitory neurons there (Fig. 7*a*). We recorded from 30 imaging sites in six Vgat-ires-Cre mice.

As shown in Figure 7*b*, the proportion of inhibitory DS cells was significantly reduced ($27.3 \pm 7.7\%$ vs $14.5 \pm 8.7\%$, $p = 4.7 \times 10^{-8}$; awake vs iso; WSR test), and that of inhibitory OS cells was slightly

increased ($15.2 \pm 5.2\%$ vs $21.1 \pm 11.7\%$; awake vs iso, $p = 0.0081$) during isoflurane anesthesia. There was no change in the proportion of nonselective neurons ($60.2 \pm 10.5\%$ vs $62.6 \pm 16.5\%$, $p = 0.25$). We further examined the distributions of DSI and OSI values during awake and isoflurane conditions. For 217 neurons with responses in an example imaging site, the distribution of DSIs was significantly lower during isoflurane conditions ($p = 0.045$, KS test; Fig. 7*c*), while that of OSIs did not change ($p = 0.45$; Fig. 7*f*). Similar tendencies were also observed in the cumulative distributions of 4942 inhibitory neurons from 30 imaging sites (DSI, $p = 2.2 \times 10^{-16}$; OSI, $p = 1.8 \times 10^{-11}$; Fig. 7*d,g*). Similar to the distributions of DSIs and OSIs, the mean DSI and OSI of individual imaging sites ($n = 30$) indicated that isoflurane reduced direction selectivity of the inhibitory neurons (DSI: 0.137 ± 0.029 vs 0.098 ± 0.030 ; awake vs iso; $p = 4.7 \times 10^{-7}$, WSR test; Fig. 7*e*). Isoflurane increased the orientation selectivity, but the effect was smaller (OSI: 0.092 ± 0.012 vs 0.099 ± 0.029 ; awake vs iso, $p = 0.096$; Fig. 7*h*). Changes in tuning properties of inhibitory DS cells and inhibitory OS cells from an example imaging plane are shown in Figure 7, *i* and *j*. In this imaging site, 50 DS cells and 27 OS cells were observed during the awake condition (Fig. 7*i, j*, left panels). During isoflurane anesthesia, 34 DS cells and 39 OS cells were detected (Fig. 7*i, j*, right panels). Similar to the results from the whole population (Figs. 3, 4, 6), isoflurane altered both the direction and orientation selectivity of individual inhibitory neurons.

The randomness of the clusters of inhibitory population was also analyzed in the same way as for the whole population. In a comparison of the awake data with the randomized dataset, a significant clustering was observed in inhibitory DS cells located within 200 μm [Fig. 7*o*: RND (green) vs awake (red); 0–100 μm : $p = 0.0022$, $n = 30$; 100–200 μm : $p = 3.2$, $n = 30$; 200–300 μm : $p = 0.11$, $n = 30$; WSR test]. Furthermore, comparing preferred directions of DS cells during the awake and iso conditions, showed that inhibitory DS cells exhibited stronger clustering patterns during the isoflurane condition [Fig. 7*o*: awake (red) vs iso

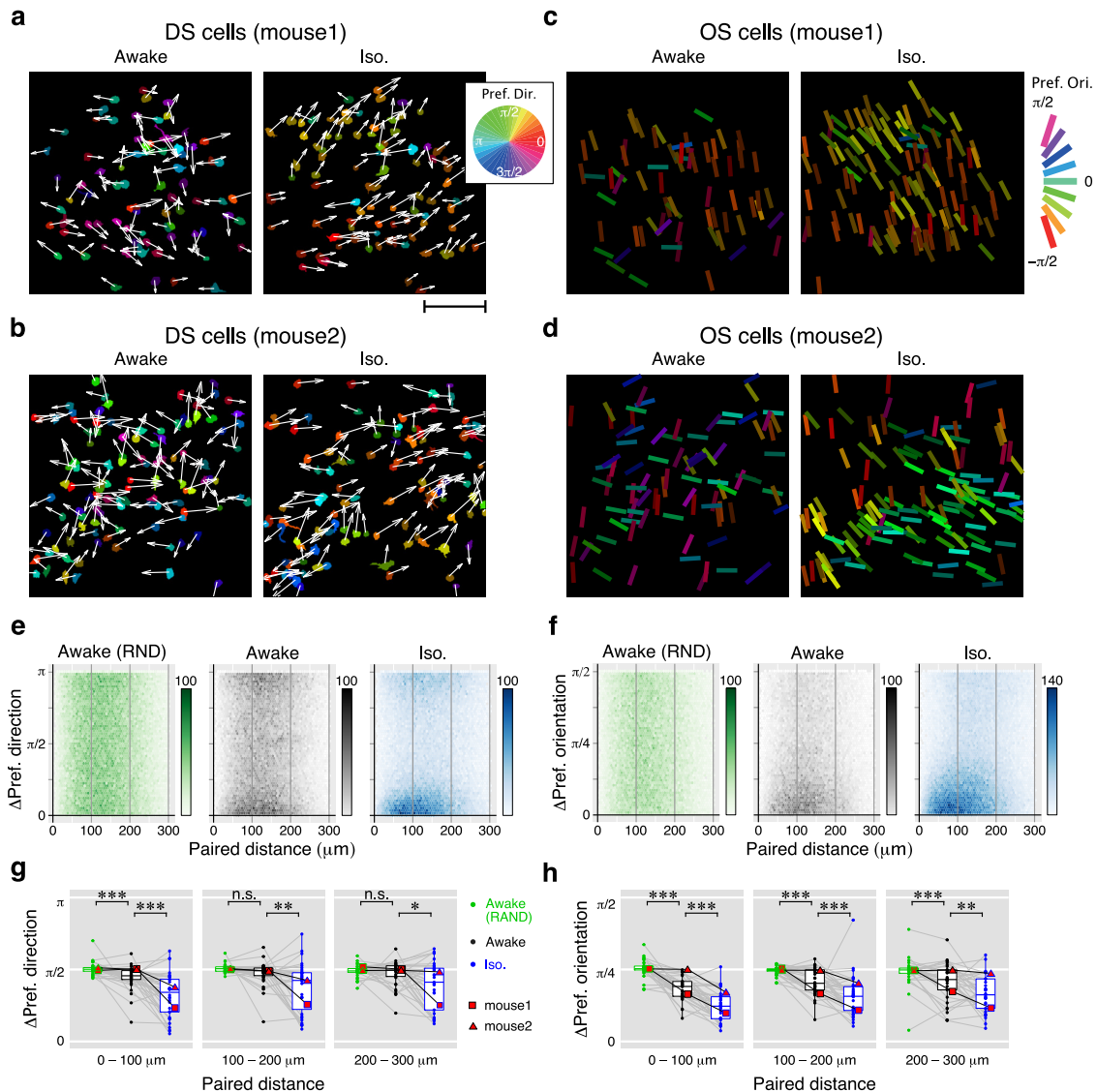


Figure 6. Local similarities of direction and orientation-selective neurons. **a, b**, Locations of DS cells in two example imaging sites from different mice. The direction of the arrows and the colors of the ROIs indicate the preferred directions of the cells. Results from awake and iso conditions are shown in the left and right panels, respectively. Scale bar: **a**, 100 μm. **c, d**, Locations of OS cells in two imaging sites. Bar angles and colors indicate the preferred orientations. The centers of each bar represent the centers of each ROI. **e, f**, 2-D histograms of the absolute differences in the preferred directions (**e**) or preferred orientations (**f**) versus the horizontal distance of all pairs of neurons from 35 imaging sites. The color intensity of each dot indicates the number of pairs according to the scale shown to the right. **g, h**, Comparison of local similarity of the preferred direction (**g**) and the preferred orientation (**h**) of cells in the RND (green), awake (black), and iso (blue) conditions. Dots indicate the mean differences of preferred directions from each imaging site for each 100 μm step in the distance of the neuron pairs. Data from example mice (**a–d**) are shown with red squares (mouse 1) and triangles (mouse 2). n.s.: not significant.

(pink); 0–100 μm: $p = 7.7 \times 10^{-7}$, $n = 29$; 100–200 μm: $p = 4.1 \times 10^{-7}$, $n = 29$; 200–300 μm: $p = 1.1 \times 10^{-4}$, $n = 28$). Similar to the inhibitory DS cells, clustered localization of inhibitory OS cells was observed during the awake condition [Fig. 7*p*: randomized (green) vs awake (red); 0–100 μm: $p = 1.3 \times 10^{-7}$, $n = 30$; 100–200 μm: $p = 9.9 \times 10^{-5}$, $n = 30$; 200–300 μm: $p = 0.57$, $n = 30$). The local similarities of inhibitory OS cells were also higher during the isoflurane condition than the awake conditions [Fig. 7*p*: awake (red) vs iso (pink); 0–100 μm: $p = 1.2 \times 10^{-5}$, $n = 29$; 100–200 μm: $p = 2.4 \times 10^{-6}$, $n = 29$; 200–300 μm: $p = 5.7 \times 10^{-6}$, $n = 28$].

Inhibitory responses at null direction were reduced by isoflurane

Compared with results from the whole-cell population (Fig. 3*a–d*), the strength of the direction selectivity of inhibitory sSC

neurons was significantly reduced by isoflurane anesthesia (Fig. 7*b–e*). To examine whether these effects could be observed in Ca^{2+} responses to the moving-bar stimuli, suppressive responses during the moving-bar stimulation were measured. In some DS cells, suppressive fluorescent changes were observed at the null direction, which is opposite the preferred direction. Color maps in Figure 8, *a* and *b*, illustrate the $\Delta F/F_0$ of 108 DS cells in the awake condition (left) and 102 DS cells under isoflurane anesthesia (right) recorded from the same imaging site. The *x*-axes in both panels are sorted as a function of difference from the preferred directions (indicated as “0” rad). Suppressing fluorescent changes (blueish areas) were observed particularly around the null direction (indicated as “+ π ” rad), in the awake condition. During isoflurane anesthesia, on the other hand, these suppressive responses were smaller. To compare the effects of isoflurane on both excitatory responses at the preferred direction and

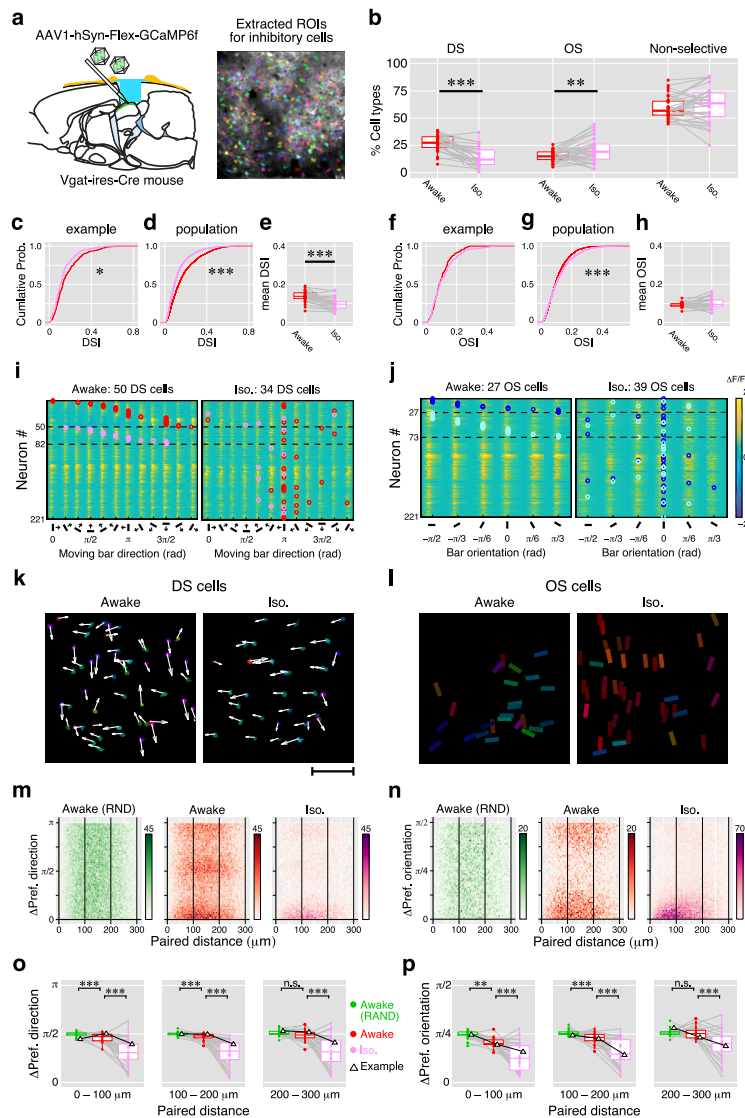


Figure 7. Summary of isoflurane effects on direction and orientation responses of inhibitory sSC neurons. **a**, Cre-dependent GCaMP expression into the inhibitory neurons and the extracted ROI image. **b**, Proportions of DS cells, OS cells, and nonselective cells. Dots indicate the mean proportions of the three response types in awake (red) and iso (pink) conditions recorded from 30 imaging sites. Gray lines indicate each pair (awake vs iso). **c–e**, Changes in the DSI. **c**, The cumulative probability of DSI in an example site (awake, 217 cells; iso, 204 cells). **d**, The cumulative probability of DSI in 30 imaging sites (awake, 5213 cells; iso, 4568 cells). **e**, Comparison of changes in mean DSIs. Dots indicate the individual mean DSI from 30 imaging sites. **f–h**, Changes in OSI are shown with cumulative probabilities and paired comparison of mean OSIs, as in **c** and **d**. Red symbols indicate the data from the awake condition, and pink symbols indicate those from the isoflurane condition. Gray lines connect paired data (awake vs iso). **i, j**, Color maps show the averaged Ca^{2+} responses to 12 moving-bar stimuli of 221 inhibitory neurons recorded from an example imaging site (DS responses, **i**; OS responses, **j**). **k**, Locations of the DS cells shown in **i** mapped onto the field of view. Scale bar, 100 μm . **l**, Locations of the OS cells shown in **j**. Arrows and bar angles indicate their preferred direction and orientation, respectively, using the same format shown in Figure 5. **m, n**, 2-D histograms of the absolute differences in the preferred directions (**m**) or preferred orientations (**n**) versus horizontal distance of all pairs of inhibitory neurons from 30 imaging sites. The color intensity of each dot indicates the number of pairs according to the scale shown to the right. **o, p**, Comparison of local similarity of the preferred direction (**o**) and preferred orientation (**p**) of cells in the RND (green), awake (red), and iso (pink) conditions. Dots indicate the mean differences of preferred directions from each imaging site for each 100 μm step in the distance of the neuron pairs. Data from the example mouse (**i–l**) are shown with triangles. n.s.: not significant.

suppressive responses near the null direction, we compared mean amplitudes of the maximum fluorescence changes at the preferred direction (peak) and mean amplitudes of the negative fluorescence changes at the null direction (trough), as shown in Figure 8c. There were no differences in peak response amplitudes (Fig. 8d) between the awake and isoflurane conditions for both the whole population (awake vs iso; 1.99 ± 0.59 vs 2.05 ± 0.77 ,

$p = 0.79$) and the inhibitory neuronal population (1.84 ± 0.35 vs 1.83 ± 0.55 , $p = 0.89$). On the other hand, trough amplitudes (Fig. 8e) were significantly decreased during isoflurane conditions for both the whole population (0.23 ± 0.07 vs 0.16 ± 0.06 , $p = 3.2 \times 10^{-8}$) and the inhibitory population (0.24 ± 0.06 vs 0.17 ± 0.08 , $p = 2.3 \times 10^{-4}$). This observation suggests that both excitatory and inhibitory DS cells received inhibitory inputs when the stimulus was moving in the null direction during the awake condition, while these inhibitory interactions decreased during isoflurane anesthesia.

Discussion

This study has shown that both the direction and orientation selectivity of sSC neurons are changed by light isoflurane anesthesia. Both at the population and individual neuronal levels, tuning properties were strongly affected by isoflurane. The effects of isoflurane on individual sSC neurons, however, were diverse. We observed that many neurons that showed weak selectivity in the awake condition became DS and/or OS cells during isoflurane anesthesia. At the same time, some DS or OS cells became less selective during isoflurane anesthesia. Furthermore, under isoflurane anesthesia, a prominent cluster-like DS and OS cell organization was observed. In the awake condition, the local clustering of OS cells was limited to within 100 μm of paired distance and became even stronger during isoflurane. Similar results were found in the inhibitory neuron population.

Recent imaging studies demonstrated in awake animals that motion direction-selective and orientation-selective neurons in the sSC form the patchy map or columnar organization that occupies a relatively large area of the retinotopic map (Feinberg and Meister, 2015; Li et al., 2020). The preferences of OS cells were also shown to be dependent on their retinotopic location in the sSC, suggesting that their preferred orientations are arranged in parallel in a concentric circle around the central visual field, particularly at the peripheral visual field (Ahmadlou and Heimel, 2015; de Malmazet et al., 2018). However, other studies pointed out that the correlation between retinotopic position and feature selectivity of sSC neurons was not always consistent, but rather, that the map-like pattern appeared to be more ambiguous (Inayat et al., 2015; Savier et al.,

2019; Chen et al., 2021). Our current results showed that the map-like representation of orientation and/or direction selectivity was affected by light isoflurane anesthesia, at least in the area approximately $\pm 20^\circ$ from the center of the visual field, suggesting that functional maps in the sSC can be dynamically changed in particular situations.

An important factor that might affect spatial organization is eye movements. To check for this, we recorded eye movements at 500 Hz to detect fast, saccade-like eye movements, OKRs, or unintentional rotations of the eyeball during the experiments. We did not detect any OKR-like, slow eye movements during presentations of moving-bar stimuli; but, as reported previously, saccade-like eye movements were observed at random times throughout the experiments (Sakatani and Isa, 2007). We excluded such trials from the analysis. Therefore, it is unlikely our findings were caused by eye movements.

The existence of functional, cluster-like architectures or columnar structure was first observed in the cerebral cortex (Mountcastle et al., 1955; Mountcastle, 1957; Hubel and Wiesel, 1965, 1968). Functional columns in the cortex are considered to enable more efficient computation by modularizing complex brain circuits. It remains unclear, however, whether such columnar-like or map-like cell architecture contributes to the efficient computation of visual processing in the SC. Usually, functional architectures are developed gradually by genetic and molecular mechanisms (Crowley and Katz, 1999), spontaneous activities (Butts and Rokhsar, 2001), and appropriate sensory stimuli received throughout the developmental stages (Triplett et al., 2009; Cang and Feldheim, 2013; Cang et al., 2018) and are considered to be stable, once formed. On the other hand, our results indicated that not only individual DS and OS neurons, but also the spatial patterns of their populations varied during isoflurane anesthesia.

We also found cell type-specific differences in the effects of isoflurane anesthesia. During isoflurane anesthesia, the direction selectivity of inhibitory cells was significantly reduced compared with that in the awake state (Fig. 6). Furthermore, while DS neurons received inhibitory input at their null direction in the awake condition, the inhibitory responses were weaker during isoflurane anesthesia (Fig. 8). This reduction in inhibitory interaction by isoflurane may have highlighted the local excitatory connections that shared retinal inputs or tuning properties. One hypothesis might be that, in the awake condition, inhibitory DS neurons provide null suppression to excitatory subnetworks. In contrast, during light isoflurane condition, those inhibitory DS neurons were suppressed (Fig. 7). This could weaken or eliminate links between local excitatory networks, possibly enabling local similarity to increase and thereby leading to the enhanced cluster-like organization in an attractor-like manner (Fig. 6). Another possible mechanism of null suppression of DS cells might originate from direction-selective retinal ganglion cell

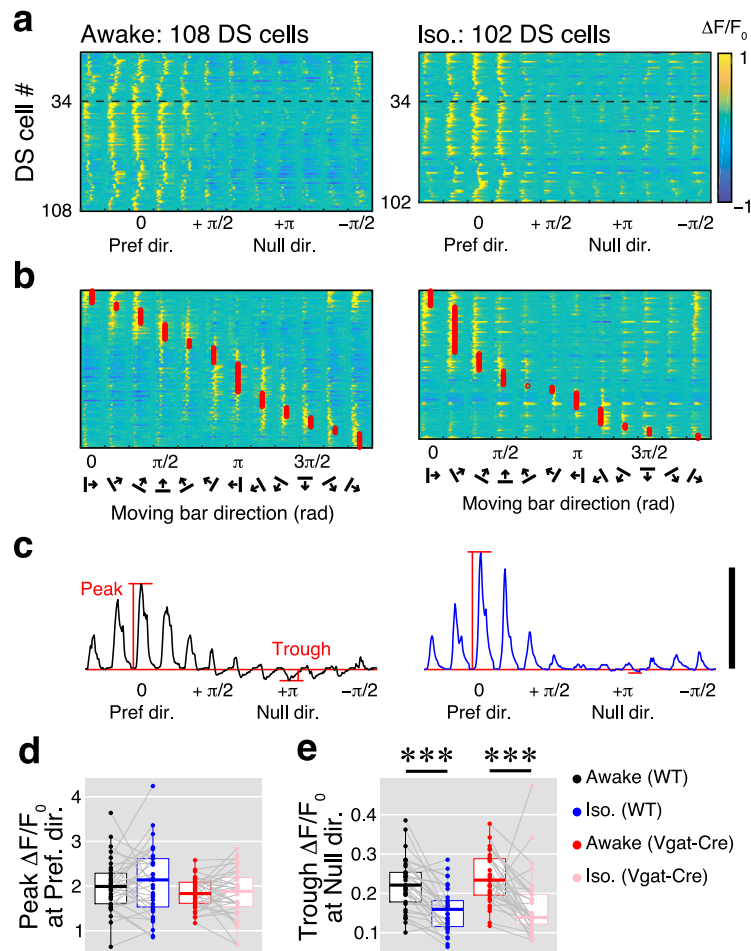


Figure 8. The inhibitory effect of isoflurane on responses in the null direction of DS cells. **a**, Color maps indicate Ca^{2+} responses of 108 DS cells in the awake condition (left) and 102 DS cells under isoflurane anesthesia (right) from the same example imaging site. The amplitude of the $\Delta F/F_0$ is color coded according to the color bar to the right. Responses are aligned by the preferred direction of individual DS cells at 0 in the x-axis. Thirty-four neurons above the dotted line showed direction selectivity in both conditions. **b**, The same neurons recorded in **a** are shown as a function of stimulus directions (approximate preferred directions are indicated by red circles). **c**, Averaged $\Delta F/F_0$ traces of 108 DS cells in the awake condition (left) and 102 DS cells under isoflurane anesthesia (right). Horizontal red lines are the baselines. Calibration: 1 $\Delta F/F_0$. **d**, **e**, Comparisons of peak (**d**) and trough (**e**) amplitudes of the awake and isoflurane conditions. Black and blue dots are data from the wild-type mice. Red and pink are data from the inhibitory neurons in the Vgat-ires-Cre mice.

inputs (Shi et al., 2017). It is not clear whether the inhibitory response at the null directions is mediated by mutual connections of inhibitory DS neurons within the sSC or is provided by other brain regions. Direct inputs from inhibitory retinal ganglion cells, which are thought to project to the SC (Luo et al., 2020), may also be involved in mediating the null suppression.

Other anesthetics, such as a mixture of ketamine-xylazine or urethane, did not cause drastic changes in the tuning properties of SC neurons or the spatial properties of their functional map (Chen et al., 2021). We also tested ketamine-xylazine anesthesia but did not observe the consistent changes in spatial patterns of DS and OS responses seen in this study (data not shown), which suggests that the enhanced pattern of DS and OS organization was specific to isoflurane anesthesia. Different mechanisms of action of these anesthetics may underlie the observed enhancement of local similarity of DS/OS cells. Ketamine reduces excitatory inputs by antagonizing NMDA receptors. Isoflurane, on the other hand, activates GABA_A receptors. Disrupting local inhibitory network by isoflurane might result in changing spatial

properties of the DS and OS maps. Isoflurane has been reported to have diverse effects on the response properties of neurons in different brain areas. For example, in the auditory midbrain, the spectral tuning selectivity of excitatory neurons was reduced, while that of the inhibitory neurons was not (Chen and Song, 2019). In layer 2/3 neurons in mouse V1, isoflurane reduced direction selectivity, while orientation selectivity was not affected (Goltstein et al., 2015), which is similar to our results from inhibitory SC neurons. However, cortical inputs might not change feature-selective responses of SC neurons (Michael, 1970; Zhao et al., 2014); thus, the retinal inputs or the local network within the SC might be affected more directly by isoflurane. In addition to direct effects on the excitatory versus inhibitory balance in the local circuits, the sSC also receives extrinsic inputs from not only visual systems but also from neuromodulatory systems, such as acetylcholine (Graybiel, 1978; Tokuoka et al., 2020) and dopamine (Bolton et al., 2015; Montardy et al., 2021). Thus, the network property may have been indirectly altered because of changes in its dependence on sensory inputs or sensitivity to these modulators.

To reveal the mechanisms by which the direction and orientation selectivity of the sSC neurons are generated and modulated by brain state, more detailed local circuit models are necessary. The sSC consists of several different cell types, which are differentiated by morphology, intrinsic membrane properties, genetic markers, and their projection targets (Langer and Lund, 1974; May, 2006; Isa and Hall, 2009; Gale and Murphy, 2014, 2016, 2018). The present study revealed the complexity of the effect of isoflurane on tuning properties of individual cell types. Although the percentage of DS cells in the entire cell population did not change, the percentage of DS cells among inhibitory neurons decreased, suggesting that the proportion of DS cells among excitatory neurons probably increased. Future studies of excitatory cell-specific changes are necessary for clarifying the mechanism of DS/OS properties in the sSC.

The physiological roles of direction and orientation maps in the sSC are still unclear. The important insight of the present study is that they might depend on brain states. An interesting concept was proposed by de Malmazet et al. (2018). They reported that DS cells whose preferred direction was biased to the nasal-to-temporal direction in the awake state were localized in the binocular region. This direction matched the optic flow when mice moved forward, suggesting that the binocular area in the sSC might help with the detection of self-motions. However, extracting specific types of information in only a specific region on the retinotopic map implies that other types of information might be ignored or missed and not be transported downstream from the sSC. As our results show, the spatial randomness of DS and OS tuning is high in the awake state, indicating that the sSC might be controlled to reduce the loss of information by preventing an extreme concentration of cells with similar tuning properties on a large part of the retinotopic map. Further studies using cell type-specific or circuit-specific manipulations combined with large-scale recording will reveal physiological roles of the functional architectures in the sSC.

References

- Agostinelli C, Lund U (2017) R package circular: circular statistics (version 0.4-93). Vienna: R Foundation for Statistical Computing.
- Ahmadlou M, Heimel JA (2015) Preference for concentric orientations in the mouse superior colliculus. *Nat Commun* 6:6773.
- Ajina S, Pollard M, Bridge H (2020) The superior colliculus and amygdala support evaluation of face trait in blindsight. *Front Neurol* 11:769.
- Anzai A, Peng X, Van Essen DC (2007) Neurons in monkey visual area V2 encode combinations of orientations. *Nat Neurosci* 10:1313–1321.
- Basso MA, Bickford ME, Cang J (2021) Unraveling circuits of visual perception and cognition through the superior colliculus. *Neuron* 109:918–937.
- Behan M, Steinhacker K, Jeffrey-Borger S, Meredith MA (2002) Chemoarchitecture of GABAergic neurons in the ferret superior colliculus. *J Comp Neurol* 452:334–359.
- Bieda MC, Su H, Maciver MB (2009) Anesthetics discriminate between tonic and phasic gamma-aminobutyric acid receptors on hippocampal CA1 neurons. *Anesth Analg* 108:484–490.
- Bolton AD, Murata Y, Kirchner R, Kim SY, Young A, Dang T, Yanagawa Y, Constantine-Paton M (2015) A diencephalic dopamine source provides input to the superior colliculus, where D1 and D2 receptors segregate to distinct functional zones. *Cell Rep* 13:1003–1015.
- Brainard DH (1997) The Psychophysics Toolbox. *Spat Vis* 10:433–436.
- Bukhari Q, Schroeter A, Rudin M (2018) Increasing isoflurane dose reduces homotopic correlation and functional segregation of brain networks in mice as revealed by resting-state fMRI. *Sci Rep* 8:10591.
- Butts DA, Rokhsar DS (2001) The information content of spontaneous retinal waves. *J Neurosci* 21:961–973.
- Cang J, Feldheim DA (2013) Developmental mechanisms of topographic map formation and alignment. *Annu Rev Neurosci* 36:51–77.
- Cang J, Savier E, Barchini J, Liu X (2018) Visual function, organization, and development of the mouse superior colliculus. *Annu Rev Vis Sci* 4:239–262.
- Chang JT, Fitzpatrick D (2021) Development of visual response selectivity in cortical GABAergic interneurons. *bioRxiv* 453281. doi:10.1101/2021.07.21.453281.
- Chen C, Song S (2019) Differential cell-type dependent brain state modulations of sensory representations in the non-lemniscal mouse inferior colliculus. *Commun Biol* 2:356.
- Chen H, Savier EL, DePiero VJ, Cang J (2021) Lack of evidence for stereotypical direction columns in the mouse superior colliculus. *J Neurosci* 41:461–473.
- Chen T-W, Wardill TJ, Sun Y, Pulver SR, Renninger SL, Baohan A, Schreier ER, Kerr RA, Orger MB, Jayaraman V, Looger LL, Svoboda K, Kim DS (2013) Ultrasensitive fluorescent proteins for imaging neuronal activity. *Nature* 499:295–300.
- Crowley JC, Katz LC (1999) Development of ocular dominance columns in the absence of retinal input. *Nat Neurosci* 2:1125–1130.
- de Gelder B, Morris JS, Dolan RJ (2005) Unconscious fear influences emotional awareness of faces and voices. *Proc Natl Acad Sci U S A* 102:18682–18687.
- de Malmazet D, Kühn NK, Farrow K (2018) Retinotopic separation of nasal and temporal motion selectivity in the mouse superior colliculus. *Curr Biol* 28:2961–2969.e4.
- Dräger UC, Hubel DH (1976) Topography of visual and somatosensory projections to mouse superior colliculus. *J Neurophysiol* 39:91–101.
- Feinberg EH, Meister M (2015) Orientation columns in the mouse superior colliculus. *Nature* 519:229–232.
- Gale SD, Murphy GJ (2014) Distinct representation and distribution of visual information by specific cell types in mouse superficial superior colliculus. *J Neurosci* 34:13458–13471.
- Gale SD, Murphy GJ (2016) Active dendritic properties and local inhibitory input enable selectivity for object motion in mouse superior colliculus neurons. *J Neurosci* 36:9111–9123.
- Gale SD, Murphy GJ (2018) Distinct cell types in the superficial superior colliculus project to the dorsal lateral geniculate and lateral posterior thalamic nuclei. *J Neurophysiol* 120:1286–1292.
- Goltstein PM, Montijn JS, Pennartz CMA (2015) Effects of isoflurane anesthesia on ensemble patterns of Ca²⁺ activity in mouse V1: reduced direction selectivity independent of increased correlations in cellular activity. *PLoS One* 10:e0118277.
- Graybiel AM (1978) A satellite system of the superior colliculus: the parabrachial nucleus and its projections to the superficial collicular layers. *Brain Res* 145:365–374.
- Hoy JL, Bishop HI, Niell CM (2019) Defined cell types in superior colliculus make distinct contributions to prey capture behavior in the mouse. *Curr Biol* 29:4130–4138.
- Hubel DH, Wiesel TN (1965) Receptive fields and functional architecture in two nonstriate visual areas (18 and 19) of the cat. *J Neurophysiol* 28:229–289.

- Hubel DH, Wiesel TN (1968) Receptive fields and functional architecture of monkey striate cortex. *J Physiol* 195:215–243.
- Inayat S, Barchini J, Chen H, Feng L, Liu X, Cang J (2015) Neurons in the most superficial lamina of the mouse superior colliculus are highly selective for stimulus direction. *J Neurosci* 35:7992–8003.
- Isa K, Sooksawat T, Kobayashi K, Kobayashi K, Redgrave P, Isa T (2020) Dissecting the tectal output channels for orienting and defense responses. *eNeuro* 7:ENEURO.0271-20.2020.
- Isa T, Hall WC (2009) Exploring the superior colliculus in vitro. *J Neurophysiol* 102:2581–2593.
- Isa T, Marquez-Legorreta E, Grillner S, Scott EK (2021) The tectum/superior colliculus as the vertebrate solution for spatial sensory integration and action. *Curr Biol* 31:R741–R762.
- Jin J, Wang Y, Swadlow HA, Alonso JM (2011) Population receptive fields of ON and OFF thalamic inputs to an orientation column in visual cortex. *Nat Neurosci* 14:232–238.
- Kasai M, Isa T (2016) Imaging population dynamics of surround suppression in the superior colliculus. *Eur J Neurosci* 44:2543–2556.
- Langer TP, Lund RD (1974) The upper layers of the superior colliculus of the rat: a Golgi study. *J Comp Neurol* 158:405–435.
- Li Y-T, Turan Z, Meister M (2020) Functional architecture of motion direction in the mouse superior colliculus. *Curr Biol* 30:3304–3315.e4.
- Luo X, Cai D, Shen K, Deng Q, Lei X, Jin S, Zeng W-B, Li H, Xu F, Huang L, Ren C, Luo M-H, Xie T, Shen Y (2020) Superior colliculus-projecting GABAergic retinal ganglion cells mediate looming-evoked flight response. *bioRxiv*. Advance online publication. Retrieved December 6, 2021.
- Matsuda K, Nagami T, Sugase Y, Takemura A, Kawano K (2017) A widely applicable real-time mono/binocular eye tracking system using a high frame-rate digital camera. In: *Human-computer interaction. User interface design, development and multimodality* (Masaaki K, ed), pp 593–608. Cham, Switzerland: Springer International.
- May PJ (2006) The mammalian superior colliculus: laminar structure and connections. *Prog Brain Res* 151:321–378.
- Mazurek M, Kager M, Van Hooser SD (2014) Robust quantification of orientation selectivity and direction selectivity. *Front Neural Circuits* 8:92.
- Michael CR (1970) Integration of retinal and cortical information in the superior colliculus of the ground squirrel. *Brain Behav Evol* 3:205–209.
- Mize PR (1988) Immunocytochemical localization of gamma-aminobutyric acid (GABA) in the cat superior colliculus. *J Comp Neurol* 276:169–187.
- Montardy Q, Zhou Z, Li L, Yang Q, Lei Z, Feng X, Chen S, Shi Q, Zhang H, Chen S, Zhang Z, Zhao B, Xu F, Lu Z, Wang L (2021) Dopamine modulates visual threat processing in the superior colliculus via D2 receptors. *bioRxiv*. Advance online publication. Retrieved December 6, 2021. <https://doi.org/10.1101/2021.02.12.430615>.
- Mountcastle VB (1957) Modality and topographic properties of single neurons of cat's somatic sensory cortex. *J Neurophysiol* 20:408–434.
- Mountcastle VB, Berman AL, Davies PW (1955) Topographic organization and modality representation in first somatic area of cat's cerebral cortex by method of single unit analysis. *Am J Physiol* 183:10.
- Mrsic-Flogel TD, Hofer SB, Creutzfeldt C, Cloëz-Tayarani I, Changeux J-P, Bonhoeffer T, Hübener M (2005) Altered map of visual space in the superior colliculus of mice lacking early retinal waves. *J Neurosci* 25:6921–6928.
- Newman MEJ (2006) Modularity and community structure in networks. *Proc Natl Acad Sci U S A* 103:8577–8582.
- Ohki K, Chung S, Ch'ng YH, Kara P, Reid RC (2005) Functional imaging with cellular resolution reveals precise micro-architecture in visual cortex. *Nature* 433:597–603.
- Pachitariu M, Stringer C, Dipoppa M, Schröder S, Federico Rossi L, Dalgleish H, Carandini M, Harris KD (2017) Suite2p: beyond 10,000 neurons with standard two-photon microscopy. *bioRxiv*. Advance online publication. Retrieved December 6, 2021. doi:10.1101/061507.
- Pneumatikakis EA, Giovannucci A (2017) NoRMCorre: an online algorithm for piecewise rigid motion correction of calcium imaging data. *J Neurosci Methods* 291:83–94.
- Priebe NJ, Ferster D (2005) Direction selectivity of excitation and inhibition in simple cells of the cat primary visual cortex. *Neuron* 45:133–145.
- Reid RC, Alonso JM (1995) Specificity of monosynaptic connections from thalamus to visual cortex. *Nature* 378:281–284.
- Sadeh S, Rotter S (2015) Orientation selectivity in inhibition-dominated networks of spiking neurons: effect of single neuron properties and network dynamics. *PLoS Comput Biol* 11:e1004045.
- Sakatani T, Isa T (2007) Quantitative analysis of spontaneous saccade-like rapid eye movements in C57BL/6 mice. *Neurosci Res* 58:324–331.
- Savner EL, Chen H, Cang J (2019) Effects of locomotion on visual responses in the mouse superior colliculus. *J Neurosci* 39:9360–9368.
- Shang C, Liu A, Li D, Xie Z, Chen Z, Huang M, Li Y, Wang Y, Shen WL, Cao P (2019) A subcortical excitatory circuit for sensory-triggered predatory hunting in mice. *Nat Neurosci* 22:909–920.
- Shi X, Barchini J, Ledesma HA, Koren D, Jin Y, Liu X, Wei W, Cang J (2017) Retinal origin of direction selectivity in the superior colliculus. *Nat Neurosci* 20:550–558.
- Stan Development Team (2020) RStan: the R interface to Stan. R package version 2.21. <https://cran.r-project.org/web/packages/rstan/citation.html>
- Tokuoka K, Kasai M, Kobayashi K, Isa T (2020) Anatomical and electrophysiological analysis of cholinergic inputs from the parabrachial nucleus to the superficial superior colliculus. *J Neurophysiol* 124:1968–1985.
- Topf N, Jenkins A, Baron N, Harrison NL (2003) Effects of isoflurane on gamma-aminobutyric acid type A receptors activated by full and partial agonists. *Anesthesiology* 98:306–311.
- Triplet JW, Owens MT, Yamada J, Lemke G, Cang J, Stryker MP, Feldheim DA (2009) Retinal input instructs alignment of visual topographic maps. *Cell* 139:175–185.
- Vong L, Ye C, Yang Z, Choi B, Chua S Jr, Lowell BB (2011) Leptin action on GABAergic neurons prevents obesity and reduces inhibitory tone to POMC neurons. *Neuron* 71:142–154.
- Watanabe S (2010) Asymptotic equivalence of bayes cross validation and widely applicable information criterion in singular learning theory. *J Mach Learn Res* 11:3571–3594.
- Zhang X, Baer AG, Price JM, Jones PC, Garcia BJ, Romero J, Cliff AM, Mi W, Brown JB, Jacobson DA, Lydic R, Baghdoyan HA (2020) Neurotransmitter networks in mouse prefrontal cortex are reconfigured by isoflurane anesthesia. *J Neurophysiol* 123:2285–2296.
- Zhao X, Liu M, Cang J (2014) Visual cortex modulates the magnitude but not the selectivity of looming-evoked responses in the superior colliculus of awake mice. *Neuron* 84:202–213.